Control Techniques With Low Computational Burden for a DAB-Based Two-Stage DC–DC EV Charging Converter System

Nie Hou, *Member, IEEE*, Kejun Qin, *Student Member, IEEE*, Ruizhi Wei, *Student Member, IEEE*, Yue Zhang, *Member, IEEE*, and Yun Wei Li, *Fellow, IEEE*

***Abstract*—In the future, electric vehicle (EV) charging dc–dc converter systems are usually required for realizing bidirectional operation, electric isolation, and large voltage range, which can be realized at the dc stage. However, because of unavoidable reactive power, the typical bidirectional and isolated dc–dc converters, such as dual-active-bridge (DAB) dc–dc converters and *LC*-based resonant dc–dc converters, usually generate large current stress at wide-range voltage. Thus, the design cost for high-power applications will inevitably be expensive. Consequently, this article, combining a three-level buck–boost stage, adopts a DAB-based two-stage dc–dc converter with a low current stress. Then, the simple control schemes, including the soft start-up method, the linear current-control-based inner loop technique, and the soft shutdown method, are proposed for the charging of EV. Especially, based on the naturally transient behavior, the linear current-control-based inner loop technique is presented with low computational burden and without instability concern. The proposed linear technique can easily and steadily realize the charging requirements such as constant current, power, and voltage charging. Besides, the presented method has no current and voltage shoots during transient process, which can significantly enhance charging reliability. Moreover, the changing rate of a charging current can be consistent and controllable to fulfill batteries' charging requirement. Finally, experiment results are provided to verify the effectiveness of the proposed techniques.**

***Index Terms*—Electric vehicle (EV) charger, linear current control, low computational burden, low current stress.**

I. Introduction

With the appeal of carbon neutrality, the development of electric vehicles (EVs) has rapidly increased over recent years to replace fuel vehicles. From 2017 to 2022, the global EV stock has increased nearly ten times as shown in Fig. 1 [1], [2]. Along with the soaring number of EVs, there is also an exponential increase in the number of EV chargers, and the design of suitable charger converter systems and control methods become pivotal in promoting the further development of the EV industry [3].

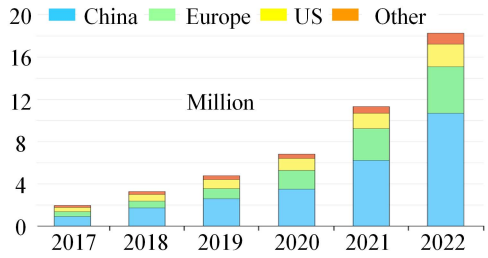

Fig. 1. Diagram of global EV stock from 2017 to 2022.

For a charger converter system, galvanic isolation with large common-mode impedance is required to minimize the leakage current and meet international standards such as IEC 62955:2018 [4], [5]. Then, the leakage current between the chassis of the charger and the earth can be less than 30mA to prevent electric shock on the human body. Moreover, according to some standards such as IEEE Std 2030.1.1-2021, a charger converter system should be able to realize the vehicle-to-grid technology, which allows an EV to have the opportunity to become not only vehicles but also mobile energy for better managing electricity resources [6], [7]. Therefore, a charger converter system should concurrently feature bidirectional and isolated abilities. Therefore, a charger converter system should concurrently feature bidirectional and isolated abilities while also having a wide output voltage range for meeting the charging requirements of different EVs [7].

The dual-active-bridge (DAB) dc–dc converter, which had been proposed in the 1990s, has become a promising candidate for the EV charging converter system due to advantages, such as bidirectional operation, electric isolation, and high-power density [8]. However, a large current stress is always generated during wide voltage conditions because of the unavoidable reactive power and the weak inertia of ac inductance. Hence, the design cost of the components such as the transformer and the switches will increase significantly. Although some advanced modulations can partly restrict the current stress [9], the improvement is still insufficient when the output-voltage change is close to 1000 V. Similarly, an *LC*-based resonant isolated

Manuscript received 4 January 2024; revised 28 April 2024; accepted 13 May 2024. Date of publication 24 May 2024; date of current version 16 July 2024. This work was supported by the Future Energy Systems initiative funding from the Canada First Research Excellence Fund. Recommended for publication by Associate Editor S. S. Williamson. *(Corresponding author: Yue Zhang.)*

The authors are with the Department of Electrical and Computer Engineering, University of Alberta, Edmonton, AB T6G 2V4, Canada (e-mail: nhou@ualberta.ca; kejun.qin@ualberta.ca; rwei4@ualberta.ca; yue30@ualberta.ca; yunwei.li@ualberta.ca).

Color versions of one or more figures in this article are available at https://doi.org/10.1109/TPEL.2024.3405193.

Digital Object Identifier 10.1109/TPEL.2024.3405193

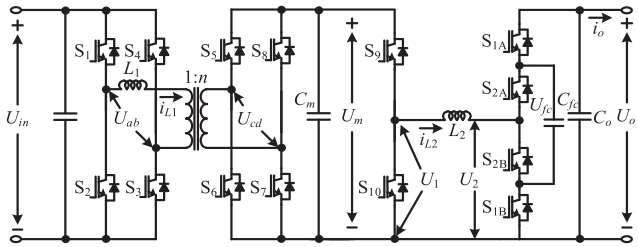

Fig. 2. Topology of the DAB-based two-stage DC–DC converter system.

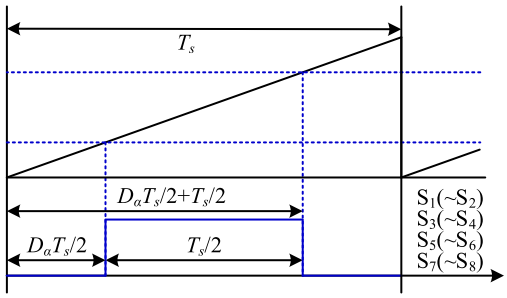

Fig. 3. Operation of the phase-shift modulator.

dc–dc converter often faces the same issue as a DAB; however, by combining a buck or boost stage, the two-stage dc–dc charger converter system can usually achieve low current stress with a wide voltage range [10], [11]. Therefore, combining a three-level buck–boost converter, a DAB-based two-stage dc–dc converter system with bidirectional operation, electric isolation, and a large voltage range is selected for forming the charger converter system in this article, as shown in Fig. 2.

On the other hand, the control strategies for realizing the start-up operation, the charging process, and the shut-down control are nevertheless crucial. In high-power applications, there is usually relatively large current and voltage margins for safety concerns because of the current or voltage overshoots during a transient process [12]. So, it is important to achieve the start-up and shut-down procedures by coordinating this DAB-based two-stage converter system to avoid potential large inrush current or voltage spike [13]. Besides, during the charging process, by using the PI-based controllers, overintegration in the control loop is usually inevitable, which results in significant overshoots even with optimized parameters [14], [15], [16]. Then, the inrush change of the output current may occur, which is unfriendly to batteries [17]. Moreover, some advanced control schemes such as the model-predictive-control (MPC) method have been proposed to restrict the dynamic overshoots of dc–dc converters [18], [19]. However, these advanced control schemes are usually sensitive to measurement noises, which limits the practical application of these methods due to reliability concerns. A natural transient-behavior-based control theory is proposed for the DAB-based two-stage dc–dc converter, but the analysis and discussion are not in detail [20].

Therefore, based on the natural transient-behavior-based control theory, a simple linear current-control-based inner loop technique is presented with a low computational burden for this adopted DAB-based two-stage dc–dc converter system. Based on this scheme, the charging requirements, such as constant current charging, constant power charging, and constant voltage charging can be realized. Moreover, the soft start-up method and the soft shutdown method are both proposed for reliable charging missions. Circuit characteristics of this converter system are analyzed in Section II. Then, the soft start-up method, the linear current-control-based inner loop technique, and the soft shut-down method are proposed for realizing the charging mission of EVs in Section III. Furthermore, the transient analysis of the presented linear current-control-based inner loop technique is presented in Section IV, which helps to design the control period. Based on the experiment results, the effectiveness of the proposed schemes is verified in Section V. Finally, Section VI concludes this article.

II. Characteristic Analysis for the Two-Stage DC–DC Converter

In this section, the unique transferred characteristics of a DAB dc–dc stage and a buck–boost stage will be analyzed, which is the foundation for designing the control system of these converters. For the DAB stage, the linear current transmission peculiarity is discussed, and for the buck–boost stage, the voltage following peculiarity is analyzed.

A. DAB DC–DC Stage

To realize current transmission, phase-shift modulation is the most popular method for DAB dc–dc converters. The phase-shift modulator for implementing the phase-shift modulation method is shown in Fig. 3. Moreover, D_α includes D_1, D_2, D_3, and D_4, which are used to realize the phase-shift operation of S_1, S_3, S_5, and S_7, respectively. Besides, T_s is the switching period. Then, based on the phase-shift modulator in Fig. 3, the whole phase-shift modulation methods for the DAB dc–dc stage can be realized.

When both-side voltages of the DAB converter are matched, minimum current stress and soft-switching performance can be realized for the converter [21]. So, in the DAB-based two-stage dc–dc converter system, the DAB dc–dc stage is employed as the voltage follower. Then, this stage is used to obtain electric isolation. Moreover, when both-side voltages are matched, an SPS modulation method, as shown in Fig. 4, with a simple operation is sufficient for realizing the current transmission of the DAB converter.

In Fig. 4, D_p is the phase-shift ratio for achieving a positive power transmission, and D_n is the phase-shift ratio for realizing a negative power transmission. Then, the relationship among D_α, D_p, and D_n can be expressed as

$$\begin{cases} D_3 = D_4 = D_p, D_1 = D_2 = 0 \\ D_1 = D_2 = D_n, D_3 = D_4 = 0 \end{cases}. \tag{1}$$

Subsequently, the transferred power of the DAB stage can be obtained as

$$P = \begin{cases} \frac{U_{\text{in}} U_m D_p (1-D_p) T_s}{2nL} & (D_p \neq 0, D_n = 0) \\ \frac{-U_{\text{in}} U_m D_n (1-D_n) T_s}{2nL} & (D_p = 0, D_n \neq 0) \end{cases}. \tag{2}$$

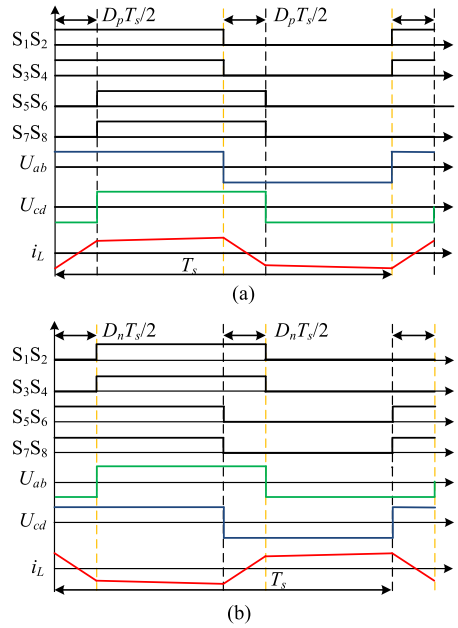

Fig. 4. SPS modulation method for DAB DC–DC stage. (a) Positive power transmission. (b) Negative power transmission.

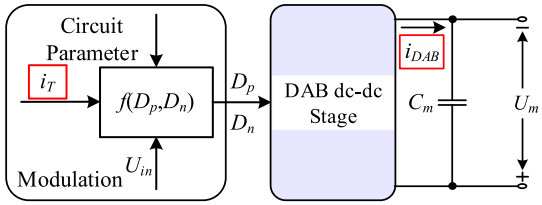

Fig. 5. Current-level modulation of the DAB DC–DC stage.

Then, according to (2), the transferred current i_T of the DAB converter under the SPS modulation method can be expressed as

$$i_T = \frac{P}{U_m} = \begin{cases} \frac{U_{\text{in}} D_p (1-D_p) T_s}{2nL} & (D_p \neq 0, D_n = 0) \\ \frac{-U_{\text{in}} D_n (1-D_n) T_s}{2nL} & (D_p = 0, D_n \neq 0) \end{cases}. \quad (3)$$

According to (3), the transferred current of the DAB converter can be directly determined by the phase-shift ratio D_p and D_n individually. So, the transition from the transferred current to the phase-shift ratio can be regarded as a part of the modulation step. Then, the current-level modulation of the DAB dc–dc converter can be realized, as shown in Fig. 5.

As shown in Fig. 5, ignoring the power loss, the output current of the DAB converter i_{DAB} should be the same as the transferred current i_T. Then, the output current of the DAB dc–dc stage i_{DAB} can be calculated as

$$i_{\text{DAB}} = i_T. \quad (4)$$

Based on (4), the relationship between the transferred current i_T and the output current i_{DAB} of the DAB dc–dc converter satisfies linear characteristic, which can help to simplify the control system design for this converter.

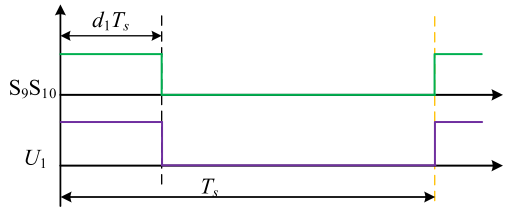

Fig. 6. Duty-ratio modulation for the buck structure.

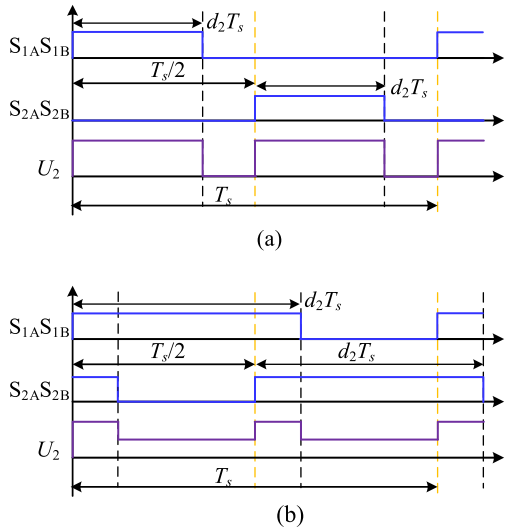

Fig. 7. Duty ratio modulation for the boost structure. (a) $d_2 \leq 0.5$. (b) $d_2 > 0.5$.

B. Three-Level Buck–Boost DC–DC Converter

In the DAB-based two-stage dc–dc converter system, the three-level buck–boost dc–dc converter can be further split into the buck structure and the three-level boost structure. The duty ratio modulation for the buck structure is illustrated in Fig. 6.

Based on Fig. 6, and ignoring the power loss, the average output voltage of the buck structure U_1 can be calculated as

$$U_1 = d_1 U_m. \quad (5)$$

Moreover, the duty ratio modulation for the three-level boost structure is demonstrated in Fig. 7. Based on Fig. 7, and ignoring the power loss, the average output voltage of the boost structure can be obtained as [22]

$$U_2 = d_2 U_o. \quad (6)$$

Combining (5) and (6), the relationship between U_m and U_o for the volt–second balance can be calculated as

$$U_m = \frac{d_2 U_o}{d_1}. \quad (7)$$

According to (7), the input voltage U_m of the three-level buck–boost dc–dc converter can be directly determined by the duty ratio d_1, the duty ratio d_2, and the output voltage U_o. With the same duty ratio, when the output voltage U_o is changed, the input voltage U_m will be changed correspondingly. So, the

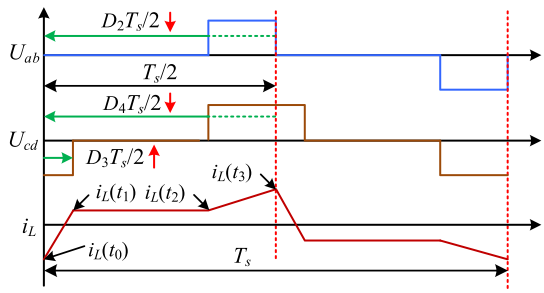

Fig. 8. TPS modulation method for realizing the soft start-up operation.

relationship between the input voltage U_m and the output voltage U_o of the three-level buck–boost converter has voltage following feature, which can be employed to simplify the control system design for this converter stage.

III. Control Techniques for the DAB-Based Two-Stage Converter System

In this section, the control techniques, including the soft start-up control method, the linear current-based inner loop control method, and the soft shutdown control method, are presented and discussed. The soft start-up control method and the soft shutdown control method are employed to realize the connection and disconnection between the charger system and an EV battery. In addition, the linear current-control-based inner loop technique can be employed to realize the constant power charger, the constant current charger, and the constant voltage charger for an EV battery.

A. Soft Start-Up Control Method

To realize the soft start-up operation of the converter system, the triple-phase-shift (TPS) modulation method is adopted to limit the current stress of the DAB dc–dc stage. The TPS modulation method for realizing the soft start-up process is illustrated in Fig. 8. As shown in Fig. 8, the phase shift ratios D_2 and D_4 are both gradually decreasing from 1, and the phase-shift ratio D_3 is gradually increasing from 0. Then, the potential maximum peak current $i_{LP\max}$ can be calculated as

$$i_{Lp\max} = \max[|i_L(t_2)|, |i_L(t_3)|]. \tag{8}$$

Based on this TPS modulation, the inductance current $i_L(t_3)$ can be expressed as

$$\begin{cases} i_L(t_3) = i_L(t_0) + \frac{(U_{\text{in}}-U_o)(1-D_2)T_s}{4L} + \frac{U_o D_3 T_s}{4L} \\ i_L(t_3) = -i_L(t_0) \end{cases}. \tag{9}$$

Then, according to (9), the inductance current $i_L(t_3)$ can be further calculated as

$$i_L(t_3) = \frac{(U_{\text{in}} - U_o)(1-D_2)T_s}{8L} + \frac{U_o D_3 T_s}{8L}. \tag{10}$$

Similarly, the inductance current $i_L(t_2)$ can be calculated as

$$i_L(t_2) = \frac{U_o D_3 T_s}{8L} - \frac{(U_{\text{in}} - U_o)(1-D_2)T_s}{8L}. \tag{11}$$

In (11), since U_o is always smaller than U_{in}, (11) can be further expressed as

$$i_L(t_2) \le \frac{U_o D_3 T_s}{8L}. \tag{12}$$

In the proposed soft start-up method, the change of the phase-shift ratio D_3 is always smaller than the change of the phase-shift ratio D_2. So, (10) can be further expressed as

$$i_L(t_3) \le \frac{U_{\text{in}}(1-D_2)T_s}{8L}. \tag{13}$$

Combing (12) and (13), the potential maximum peak current $i_{LP\max}$ can also be calculated as

$$\Delta i_{Lp\max} \le \max\left[\frac{U_o D_3 T_s}{8L}, \frac{U_{\text{in}}(1-D_2)T_s}{8L}\right]. \tag{14}$$

Then, based on (14), the potential maximum peak current $i_{LP\max}$ of the DAB stage during the start-up process can be calculated, which can be employed to limit the change of range of the phase-shift ratios D_2, D_3, and D_4. Moreover, based on the TPS modulation method shown in Fig. 8, the soft start-up process of the DAB stage can be obtained. In addition, as discussed in Section II-B, since the three-level buck–boost converter has the voltage following characteristic, the duty ratios d_1 and d_2 for realizing the soft start-up process can be calculated as

$$\begin{cases} d_1 = \frac{U_o^*}{U_m^*} = \frac{U_o^*}{U_{\text{in}}}, d_2 = 1 & (U_o^* \le U_{\text{in}}) \\ d_2 = \frac{U_m^*}{U_o^*} = \frac{U_{\text{in}}}{U_o^*}, d_1 = 1 & (U_o^* > U_{\text{in}}) \end{cases} \tag{15}$$

where U_o^* is the desired original output voltage of the converter system for connecting EV battery, and U_m^* is the desired middle voltage of the converter system. Then, combining Fig. 8 and (15), the soft start-up process of the DAB-based two-stage dc–dc converter system can be realized. During this process, the output voltage U_m of the DAB stage will be gradually increased, and the output voltage U_o and the flying capacitor voltage U_{fc} of the buck–boost stage will also be increased subsequently. When the output voltage U_o has reached its desired value, the soft start-up process is finished, and all switches can be turned OFF. In addition, the sketch diagram of the start-up process under the proposed method is shown in Fig. 9. When the soft start-up process is finished, the output voltage of the DAB stage is the same as its input voltage, and the voltage matched performance can be obtained. Besides, the required output voltage U_o for connecting EV battery can also be obtained, and the flying capacitor U_{fc} is very close to half of the output voltage. Furthermore, the charger converter system can be connected to EV battery.

B. Linear Current-Control-Based Inner Loop Technique

When the converter system is connected to the EV battery, the system can be shown in Fig. 10. Then, based on natural transient-behavior-based control theory [20], the linear current-control-based inner loop technique is presented for the DAB-based two-stage dc–dc EV charging converter system. In this method, the DAB stage can be controlled as a current source, and the buck–boost converter is employed to match the middle dc-link

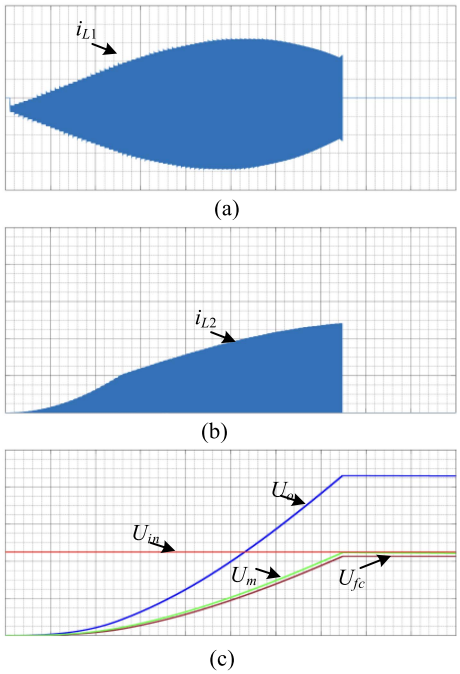

Fig. 9. Sketch diagram of the proposed soft start-up control method. (a) Inductance current i_{L1}. (b) Inductance current i_{L2}. (c) Inductance current i_{L1}.

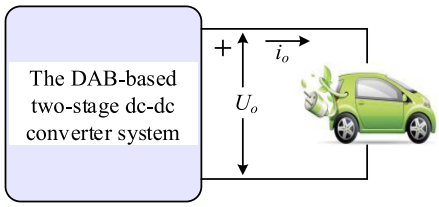

Fig. 10. Schematic diagram of the connection to EV battery.

voltage and the output voltage. Then, based on this control theory, the presented linear current-control-based inner loop technique can realize the charging requirements easily without voltage and current overshoots.

According to (3), the phase-shift ratios D_p and D_n for realizing the desired transferred current i_T can be calculated as

$$\begin{cases} D_p = \frac{1}{2} - \sqrt{\frac{l1}{4} - \frac{2nLi_T}{U_{\text{in}}T_s}} & (D_n = 0, i_T \geq 0) \\ D_n = \frac{1}{2} - \sqrt{\frac{1}{4} + \frac{2nLi_T}{U_{\text{in}}T_s}} & (D_p = 0, i_T < 0) \end{cases}. \tag{16}$$

Then, based on (16), the phase-shift ratios D_p and D_n can be obtained for realizing a certain transferred current i_T, and the DAB dc–dc stage can be easily employed as a controllable current source. Moreover, because of the voltage following characteristic, the three-level buck–boost converter can be employed to control the middle dc-link voltage U_m. Usually, this converter stage would work in buck mode or boost mode severally for low current stress. Thus, according to (15), the duty ratios d_1 and d_2 for obtaining a certain middle dc-link voltage U_m^* can be

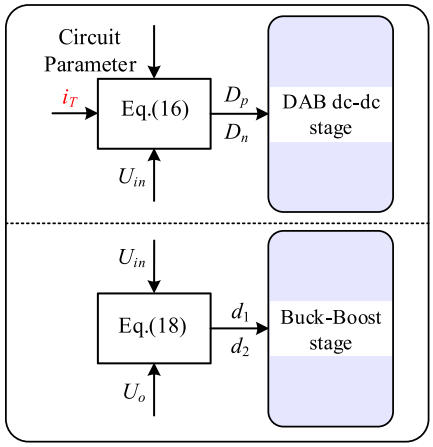

Fig. 11. Control diagram of the proposed linear current-control-based inner loop technique.

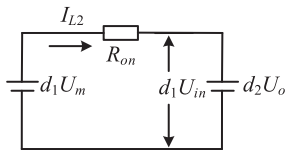

Fig. 12. Simplified average model for KVL of the three-level buck–boost stage.

calculated as

$$\begin{cases} d_1 = \frac{U_o}{U_m^*}, d_2 = 1 & (U_o \leq U_m^*) \\ d_2 = \frac{U_m^*}{U_o}, d_1 = 1 & (U_o > U_m^*) \end{cases}. \tag{17}$$

In addition, since the both-side voltages of the DAB dc–dc stage should be matched for low current stress and soft switching operation, (17) can be further expressed as

$$\begin{cases} d_1 = \frac{U_o}{U_{\text{in}}}, d_2 = 1 & (U_o \leq U_{\text{in}}) \\ d_2 = \frac{U_{\text{in}}}{U_o}, d_1 = 1 & (U_o > U_{\text{in}}) \end{cases}. \tag{18}$$

Combining (16) and (18), the linear current-control-based inner loop technique for the DAB-based two-stage dc–dc converter system can be shown in Fig. 11.

As shown in Fig. 11, the linear current-control-based inner loop technique for the DAB-based two-stage dc–dc converter system can be readily implemented. Based on the required transferred current i_T, the corresponding phase-shift ratios D_p and D_n can be calculated by (16). Moreover, based on (18), the middle dc-link voltage U_m can stabilize at the value of the input voltage U_{in}. In addition, considering the conduction resistor R_{ON} in the buck–boost stage, the simplified average model for Kirchhoff's voltage law (KVL) of this stage is demonstrated in Fig. 12.

As shown in Fig. 12, the relationship between the input voltage U_{in} and the output voltage U_m of the DAB stage can be expressed as

$$\frac{U_m}{U_{\text{in}}} = \frac{I_{L2}R_{\text{ON}}}{d_1U_{\text{in}}} + 1 \approx 1. \tag{19}$$

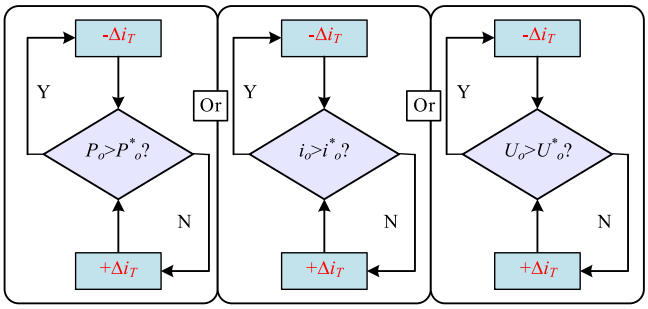

Fig. 13. Outer loop charging control scheme for different charging requirements.

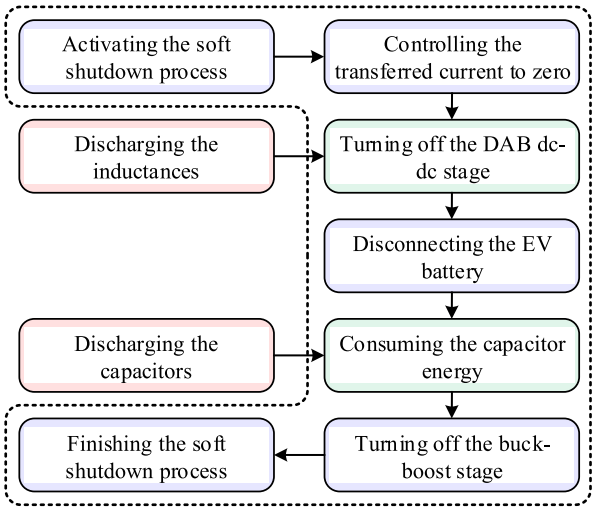

Fig. 14. Schematic diagram of the presented soft shutdown method.

For ensuring a high-efficiency performance, the conduction resistor $R_{\rm ON}$ is usually tens mΩ under high-power applications, so the equivalent voltage of the conduction resistor is far smaller than the input voltage. Even considering the conduction resistor, the middle dc-link voltage U_m should be very close to the input voltage of the DAB stage. Therefore, the voltage-matched performance of the DAB stage can be realized.

In addition, when the charger converter system is connected to an EV battery, as shown in Fig. 9, the monotonous relationship between the transferred current i_T and the charging power P_o can be ensured. Besides, the charging current i_o and the charging voltage U_o have the same relationship with the transferred current i_T. Hence, based on this linear current-control-based inner loop technique, the constant power charging, constant current charging, and constant voltage charging for the EV battery can be realized, as shown in Fig. 13.

Combining Figs. 11 and 13, the different charging requirements for the EV batteries can be realized by regulating the transferred current i_T under the proposed linear current-control-based inner loop technique. Using the constant power charging as an example, when the charging power P_o is smaller than the required value P_o^*, the transferred current i_T will be increased by Δi_T. Besides, when the charging power P_o is bigger than the required value P_o^*, the transferred current i_T will be decreased by Δi_T. Based on this principle, the change of the transferred current i_T of the DAB stage will be determined by the comparison result until the charging power P_o is the same as the required charging power P_o^*. Similarly, the constant current charging and the constant voltage charging can also be realized. Notably, between the regulation of the transferred current i_T, the steady-state condition should be obtained for the DAB-based two-stage dc–dc converter. So, there will not be voltage and current overshoots, which can boost the reliability of the charging process. In addition, without voltage and current overshoots, the utilization of switches and components will be significantly improved, which can help to reduce the cost of the converter system, especially at high-power condition.

C. Soft Shutdown Method

In this section, the soft shutdown method for the selected charging system is presented, which contains the discharging of the inductances and capacitors in the converter system and the disconnection of the EV battery. Fig. 14 shows the presented soft shutdown method for the DAB-based two-stage charging converter system. When the soft shutdown process is activated, the transferred current of the converter system should be controlled to zero at first. Then, the switches of the DAB dc–dc stage can be turned OFF, and there will not be power transferred to the EV battery. Moreover, the EV battery can be disconnected safely, without power source, and the capacitor voltages of the three-level buck–boost converter can be consumed by the conduction resistor. When the output-capacitor voltage and the middle dc-link voltage are close to zero, the switches of the buck–boost stage can be turned OFF. Moreover, except for the input capacitor, the inductance current and the capacitor voltage become zero in the DAB-based two-stage dc–dc converter system. Ultimately, the soft shutdown process is finished, and the charger converter system starts to wait for a new charging requirement.

IV. Transient Analysis of the DAB-Based Two-Stage DC–DC Converter System

In this section, the transient analysis of the adopted DAB-based two-stage dc–dc converter system is presented for determining the control period T_c of the proposed linear current-control-based inner loop technique. Then, the over integration of the control loop can be eliminated, which helps to avoid the current and voltage overshoots during transient process. Based on the proposed linear current-control-based inner loop technique, the DAB dc–dc converter acts as a controllable current source. Then, the equivalent circuit of this two-stage dc–dc converter system can be presented, as shown in Fig. 15, where R_c is the middle dc-link capacitor's resistor, and $R_{\rm eq}$ is the equivalent loss resistor of the buck–boost stage.

Based on Fig. 15, the state-space equation can be calculated as

$$\begin{cases} C_m \frac{dU_{cm}}{dt} = i_C \\ i_C = i_T - d_1 i_{L2} \\ d_1(i_C R_c + U_{cm}) = L_2 \frac{di_{L2}}{dt} + i_{L2} R_{\rm eq} + d_2 U_o \end{cases}. \quad (20)$$

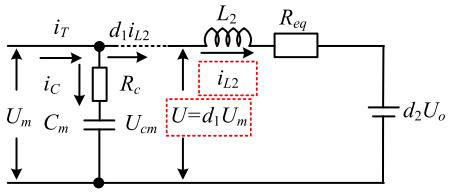

Fig. 15. Equivalent circuit of the three-level buck–boost DC–DC converter.

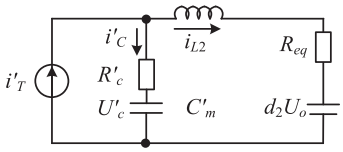

Fig. 16. Simplified circuit of the three-level buck–boost DC–DC converter.

Then, according to (20), the differential equation of the three-level buck–boost stage can be shown as

$$\frac{L_2C_m}{d_1}\frac{d^2i_{L2}}{dt^2}+\left(\frac{R_{\rm eq}C_m}{d_1}+d_1R_cC_m\right)\frac{di_{L2}}{dt}+d_1i_{L2} =i_T+R_cC_m\frac{di_T}{dt}. \tag{21}$$

According to (21), the equivalent circuit of this two-stage dc–dc converter can be depicted, as shown in Fig. 16, where i'_T, R'_c, and C'_m can be expressed as

$$\begin{cases} R'_c=d_1^2R_c \\ C'_m=\frac{C'_m}{d_1^2} \\ i'_T=\frac{i_T}{d_1} \end{cases}. \tag{22}$$

According to Fig. 16, the state-space equation of the simplified circuit can be calculated as

$$\begin{cases} C'_m\frac{dU_c}{dt}=i'_C \\ i'_C=i'_T-i_{L2} \\ R'_ci_C+U'_c=L_2\frac{di_{L2}}{dt}+i_{L2}R_{eq}+d_2U_o \end{cases}. \tag{23}$$

Based on (23), the differential equation can be obtained as

$$C'_mL_2\frac{d''i_{L2}}{dt}+(C'_mR_{eq}+C'_mR'_c)\frac{di_{L2}}{dt}+i_{L2} =i'_T+C'_mR'_c\frac{di_T}{dt}. \tag{24}$$

Since the capacitor C'_m and the resistor R'_c are far smaller than 1, (24) can be further expressed as

$$C'_mL_2\frac{d''i_{L2}}{dt}+(C'_mR_{eq}+C'_mR'_c)\frac{di_{L2}}{dt}+i_{L2}=i'_T. \tag{25}$$

Based on Laplace Transformation, the frequency-domain equation of (25) can be calculated as

$$C'_mL_2i_{L2}(s)s^2+(C'_mR_{\rm eq}+C'_mR'_c)i_{L2}(s)s+i_{L2}(s) =i'_T(s). \tag{26}$$

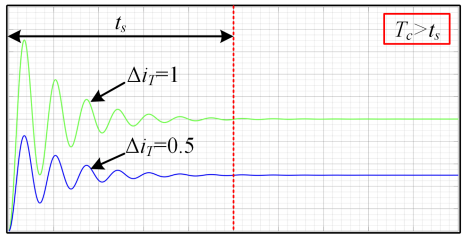

Fig. 17. Sketch diagram of the step response of the DAB-based two-stage DC–DC converter system.

Since $t_T(s)$ can be treated as a step signal under the proposed control technique, (26) can be further expressed by the change rate Δi_T as

$$C'_mL_2i_{L2}(s)s^2+(C'_mR_{\rm eq}+C'_mR'_c)i_{L2}(s)s+i_{L2}(s)=\frac{\Delta i'_T}{s}. \tag{27}$$

Then, the inductance current i_{L2}(s) can be calculated as

$$i_{L2}(s)=\Delta i'_T\left(\frac{1}{s}\frac{\frac{1}{C'_mL_2}}{s^2+\frac{(C'_mR_{\rm eq}+C'_mR'_c)}{C'_mL_2}s+\frac{1}{C'_mL_2}}\right). \tag{28}$$

Moreover, the step response in the time domain of the two-stage dc–dc converter system is expressed as

$$h(t)=\Delta i_T\left[1-\frac{1}{\sqrt{1-\zeta^2}}e^{-\zeta\omega_nt}\sin\left(\omega_n\sqrt{1-\zeta^2}t+\arccos\zeta\right)\right]. \tag{29}$$

According to (28), the natural angular frequency ω_n and damping factor ζ can be calculated as

$$\begin{cases} \omega_n=\frac{1}{\sqrt{C'_mL_2}} \\ \zeta=\frac{(C'_mR_{\rm eq}+C'_mR'_c)}{2\sqrt{C'_mL_2}} \end{cases}. \tag{30}$$

In addition, from the output side, the approximate efficiency $\eta_{\rm BB}$ of the buck–boost stage can be calculated as

$$\eta_{\rm BB}\approx\frac{d_2U_o}{i_{L2}R_{\rm eq}+d_2U_o}. \tag{31}$$

Subsequently, the approximate equivalent resistor $R_{\rm eq}$ can be expressed as

$$R_{\rm eq}\approx\frac{d_2U_o}{\eta_{\rm BB}i_{L2}}-\frac{d_2U_o}{i_{L2}}<\frac{(d_2U_o)_{\min}}{\eta_{\rm BB\,max}i_{L2\max}}-\frac{(d_2U_o)_{\min}}{i_{L2\max}}. \tag{32}$$

Furthermore, the sketch diagram of the step response under different Δi_T can be demonstrated as shown in Fig. 17. So, even with different changes, the settling time t_s of the converter system remains the same, which can be calculated as

$$t_s=\frac{\log(\sqrt{1-\zeta^2}\Delta i_{L2})-\log(\Delta i_T)}{-\zeta\omega_n}(\Delta i_{L2}<1\%\Delta i_T) \tag{33}$$

where Δi_{L2} is the tolerable inductance-current disturbance. Furthermore, the expected current disturbance Δi_{L2} should be smaller than 1% of Δi_T for achieving an approximate steady state. Then, when the control period T_c is larger than the settling time t_s, the DAB-based two-stage dc–dc converter can return to

TABLE I
CIRCUIT PARAMETERS OF THE DAB-BASED TWO-STAGE DC–DC CONVERTER SYSTEM

L_1	10 μH	f_s	20 kHz
L_2	100 μH	η_{BBmax}	98%
n	1	R_{eq}	0.1 Ω
C_m	120 μF	R_c	0.05 Ω
U_{in}	300 V	d_2	0.51
U_o	588 V	t_s	6.1 ms
i_o	-30 to 30 A	T_c	10 ms

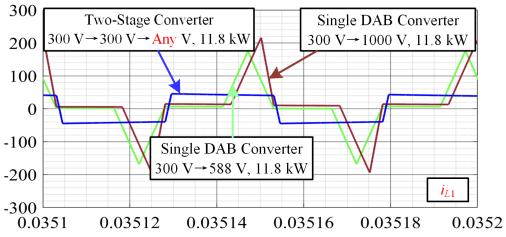

Fig. 18. Simulation results of i_{L1} with DAB-based two-stage converter and single DAB converter (i_{L1}: A; time: s).

the steady-state condition during the control period, making the general stability analysis no longer required. So, the stability of the presented linear current-control-based control scheme can be ensured for realizing the control requirements of EV battery. Besides, because the current change Δi_T in a control period is very small, there will be no current and voltage shoots by using the presented method.

V. VERIFICATION

In this section, the simulation model and the experimental platform are built to verify the effectiveness of the proposed control methods, and the main parameters of this DAB-based two-stage EV charging converter system are shown in Table I.

A. Simulation Results

Based on Simulink, the simulation model of the DAB-based two-stage dc–dc converter and the DAB dc–dc converter are built. With the same circuit parameters, simulation results of the inductance current of the DAB-based two-stage converter and the single DAB converter can be shown in Fig. 18, and the minimum peak-current modulation is applied to the single DAB converter [21]. As shown in Fig. 18, when the required output voltage is 588 or 1000 V, the peak current of the single DAB converter is four times more than that of the two-stage converter, and when the voltage difference is bigger, the peak current of the single DAB converter for the same power will be larger.

Moreover, when the DAB-based two-stage dc–dc converter is connected to the lithium-ion battery in Simulink, Fig. 19 shows the simulation results during the change between the constant-current mode and the constant-voltage mode. As shown in Fig. 19(c), the converter system is working at constant-current mode first, and the desired charging current i_o^* is 50 A. Then, the charging mode is switched to constant-voltage mode, and the

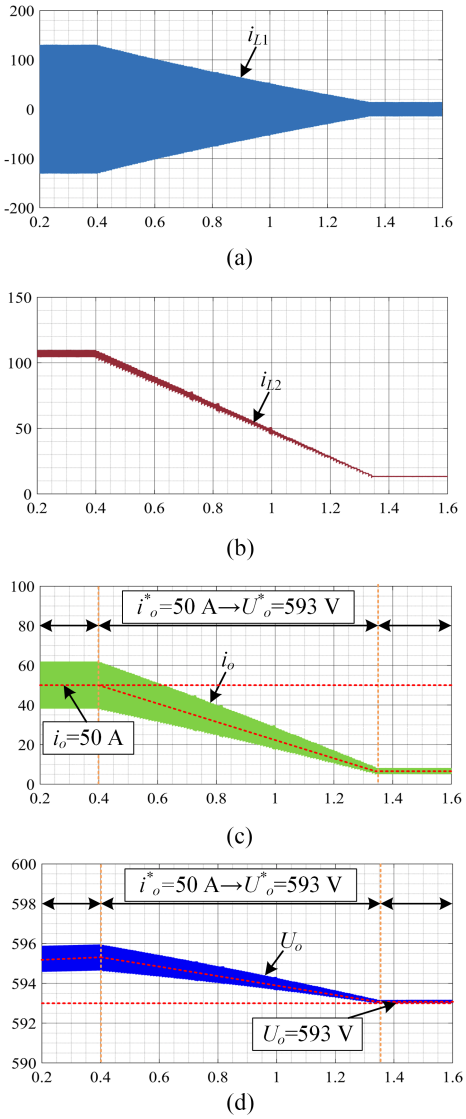

Fig. 19. Simulation results during the change of the constant-current mode and the constant-voltage mode. (i_{L1}: A; i_{L2}: A; i_o: A; U_o: V; time: s). (a) Inductance current i_{L1}. (b) Inductance current i_{L2}. (c) Output current i_o. (d) Output Voltage U_o.

desired charging voltage U_o^* is 593 V. As shown in Fig. 19(d), the required charging voltage can be obtained. Besides, as shown in Fig. 19(a)–(d), there are not any current spike and voltage spike during the transient process.

B. Experimental Results

An experiment platform of the DAB-based two-stage dc–dc converter is built to verify the proposed soft start-up method, the proposed linear current-control-based inner loop technique, and the soft shutdown method. The KEYSIGHT RP7972A is employed to act as the battery, and the REGATRON TC.GSS.32.500 is used as the input power supply. Moreover, the constant current charging is selected to verify the effectiveness of the proposed linear current-control-based inner loop technique. In addition, the picture of the platform is shown in Fig. 20.

Based on the proposed soft start-up method, the experimental results of the charger converter system can be acquired, as shown

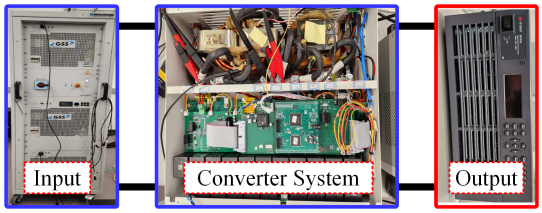

Fig. 20. Photograph of the platform.

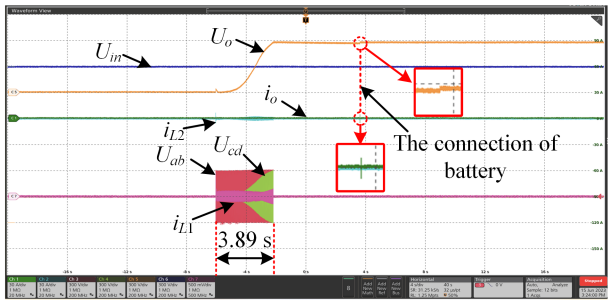

Fig. 21. Experiment results under the proposed soft start-up method ($U_{\rm in}$, U_{ab}, U_{cd}, and U_o: 300 V/div; i_{L1}: 50 A/div; i_{L2} and i_o: 30 A/div; t: 4 s/div).

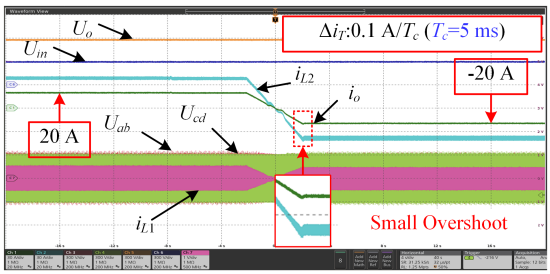

(a)

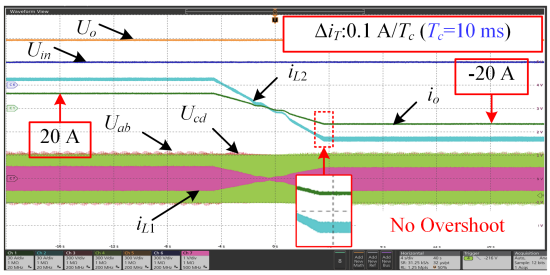

(b)

Fig. 22. Experimental results under different T_c ($U_{\rm in}$, U_{ab}, U_{cd}, and U_o: 300 V/div; i_{L1}: 100 A/div; i_{L2} and i_o: 30 A/div; t: 4 s/div). (a) $T_c = 5$ ms. (b) $T_c = 10$ ms.

in Fig. 21, where $d_1 = 1$ and $d_2 = 0.51$. When the output voltage varies from 0 to 588 V, the settling time is 3.89 s. Besides, the peak value of the ac inductance current i_{L1} is smaller than 20 A, and the dc inductance current i_{L2} is exceedingly small during the start-up process. Moreover, when the output terminal of the charger converter is connected to the battery, the spike value of the output current is about 5 A. Therefore, based on the proposed method, the soft connection of the charger converter and the battery can be achieved.

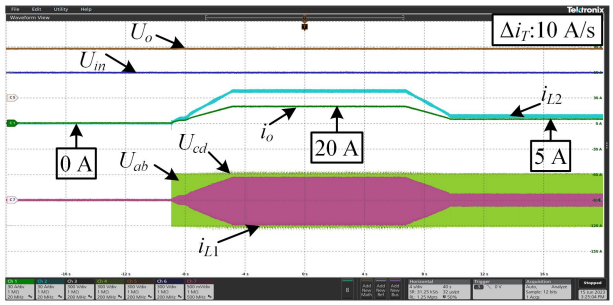

Fig. 23. Experiment results under the proposed linear current-control-based inner loop technique for constant current charging ($U_{\rm in}$, U_{ab}, U_{cd}, and U_o: 300 V/div; i_{L1}: 50 A/div; i_{L2} and i_o: 30 A/div; t: 4 s/div).

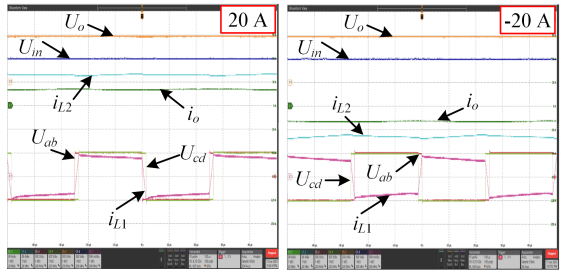

(a) (b)

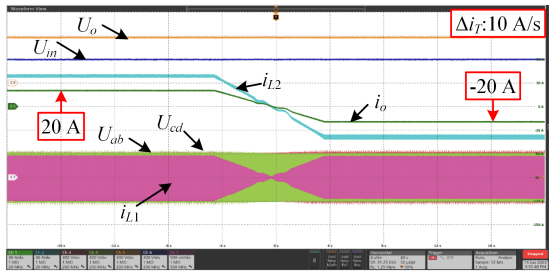

(c)

Fig. 24. Experiment results under the proposed linear current-control-based inner loop technique for bidirectional operation ($U_{\rm in}$, U_{ab}, U_{cd}, and U_o: 300 V/div; i_{L1}: 50 A/div; i_{L2} and i_o: 30 A/div; t: 4 s/div). (a) $i_o = 20$ A. (b) $i_o = -20$ A. (c) Transient process of bidirectional operation.

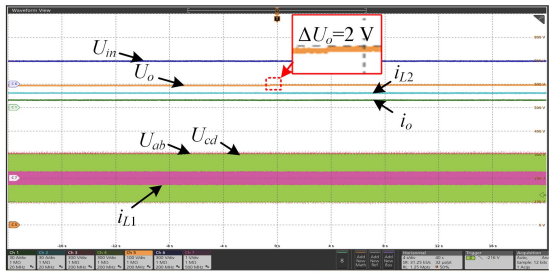

Fig. 25. Experiment results when the output voltage is changed ($U_{\rm in}$, U_{ab}, and U_{cd}: 300 V/div; U_o: 100 V/div; i_{L1}: 100 A/div; i_{L2} and i_o: 30 A/div; t: 4 s/div).

When the control period T_c is smaller or bigger than the settling time t_s, the experimental results under the presented linear current-control-based inner loop technique can be shown in Fig. 22. As shown in Fig. 22(a), when the control period T_c is smaller than the settling time t_s, the accumulated current overshoot can be observed at the end of the transient process.

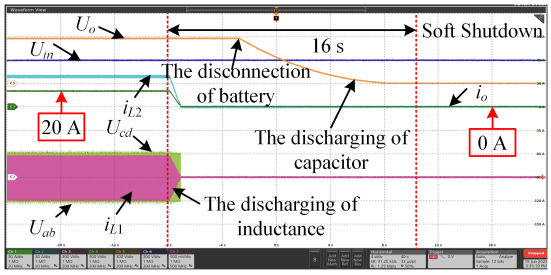

Fig. 26. Experiment results under the proposed soft shutdown method ($U_{\rm in}$, U_{ab}, U_{cd}, and U_o: 300 V/div; i_{L1}: 50 A/div; i_{L2} and i_o: 30 A/div; t: 4 s/div).

Besides, as shown in Fig. 22(b), when the control period T_c is bigger than the settling time t_s, there is not any obvious current overshoot during the transient process.

Furthermore, the experimental results of the constant current charging can be acquired, as shown in Fig. 23, where the changing rate of the transferred current i_T is 10 A/s. When the output current varies from 0 to 20 A or 20 to 5 A, the changing rate of the output current is constant, and there is no current overshoot.

Similarly, based on the proposed linear current-control-based inner loop technique, the experimental results of the bidirectional operation can be acquired, as shown in Fig. 24, where the changing rate of the transferred current i_T is 10A/s. As shown in Fig. 24(a) and (b), the zoom-in waveforms when $i_o = 20$ A or $i_o = -20$ A can be obtained. Moreover, as shown in Fig. 24(c), when the output current changes from 20 to -20 A, the changing rate of the output current is constant, and there is no current overshoot. Besides, when the output current is close to zero, there is a little change in the changing rate, which should be caused by the due time of switching signals.

Besides, when there is a sudden change of the output voltage to 2 V because of the change of battery's stage of charge, the experimental result can be shown in Fig. 25. As shown in Fig. 25, the output current can be maintained at its desired value, so the robustness of the proposed method can be ensured under output-voltage variation.

Finally, based on the proposed soft shutdown method, the experimental results of the charger converter system can be acquired, as shown in Fig. 26. First, the charging current is controlled to zero, which can realize the discharging of the ac inductance and the dc inductance. Moreover, the battery is disconnected to the charger converter, and the output capacitor voltage is consumed by the conduction resistor of the three-level buck–boost converter. When the output voltage becomes zero, the shutdown process is implemented. The total time of the shutdown process is 16 s, which can be reduced by adding a paralleled resistor for the output capacitor. Then, the charger converter system can wait for the next charging mission.

VI. Conclusion

In this article, control techniques with a low computational burden for a DAB-based two-stage dc–dc converter system are proposed for realizing the charging requirements for EV batteries. First, a soft start-up method is proposed for realizing a soft connection between the converter system and the battery. Then, based on a natural transient-behavior-based control theory, a linear current-control-based inner loop technique is presented for realizing the charging requirements of the EV battery. Moreover, a soft shutdown method is proposed for realizing the soft shutdown of the charger converter system. The conducted studies are summarized as follows.

1) Based on the soft start-up method, the required output voltage can be pre-charged for the soft connection of the battery. During the start-up process, the peak values of the inductances are minuscule. Moreover, when the charger converter system is connected to the battery, the output-current spike is also diminutive.
2) Based on the linear current-control-based inner loop technique, the changing rate of the charging current can remain constant, which is friendly to the battery. Moreover, during the transient process between different charging modes, there are no current and voltage spikes. Therefore, the reliability of the charger system can be enhanced, and the current and voltage margins of components such as inductance and switch can be reduced.
3) Based on the proposed soft shutdown method, the discharging of the inductance and the capacitor in the converter system can be realized. Then, the charger converter system can wait for the next charging mission.
4) With the transferred current as the sharing value, the proposed linear current-control-based inner loop technique can be easily employed in the paralleled system of the adopted DAB-based two-stage dc–dc converter system for higher charging power.

References

[1] United States Environmental Protection Agency, "Sources of greenhouse gas emissions," Apr. 2023. [Online]. Available: https://www.epa.gov/ghgemissions/sources-greenhouse-gas-emissions
[2] International Energy Agency, "Trends in electric light-duty vehicles," Apr. 2023. [Online]. Available: https://www.iea.org/reports/global-ev-outlook-2023/trends-in-electric-light-duty-vehicles
[3] M. Safayatullah, M. T. Elrais, S. Ghosh, R. Rezaii, and I. Batarseh, "A comprehensive review of power converter topologies and control methods for electric vehicle fast charging applications," *IEEE Access*, vol. 10, pp. 40753–40793, 2022.
[4] *Residual Direct Current Detecting Device (RDC-DD) to be Used for Mode 3 Charging of Electric Vehicles*, Standard IEC 62955:2018, IEC, Geneva, Switzerland, 2018.
[5] J. Wang et al., "Nonisolated electric vehicle chargers: Their current status and future challenges," *IEEE Electrific. Mag.*, vol. 9, no. 2, pp. 23–33, Jun. 2021.
[6] B. Sovacool, J. Kester, L. Noel, and G. Rubens, "Actors, business models, and innovation activity systems for vehicle-to-grid (V2G) technology: A comprehensive review," *Renewable Sustain. Energy Rev.*, vol. 131, Jul. 2020, Art. no. 109963.
[7] *IEEE Standard for Technical Specifications of a DC Quick and Bidirectional Charger for Use with Electric Vehicles - Redline*, IEEE Std 2030.1.1-2021, Feb. 2022.
[8] R. W. A. A. De Doncker, D. M. Divan, and M. H. Kheraluwala, "A three-phase soft-switched high-power-density DC/DC converter for high-power applications," *IEEE Trans. Ind. Appl.*, vol. 27, no. 1, pp. 63–73, Jan./Feb. 1991.
[9] N. Hou and Y. W. Li, "Overview and comparison of modulation and control strategies for a nonresonant single-phase dual-active-bridge dc–dc converter," *IEEE Trans. Power Electron.*, vol. 35, no. 3, pp. 3148–3172, Mar. 2020.
[10] B. O. Aarninkhof, D. Lyu, T. B. Soeiro, and P. Bauer, "A reconfigurable two-stage 11 kW dc–dc resonant converter for EV charging with a 150–1000 V output voltage range," *IEEE Trans. Transp. Electrific.*, vol. 10, no. 1, pp. 509–522, Mar. 2024, doi: 10.1109/TTE.2023.3279211.

[11] V. K. Goyal and A. Shukla, "Two-stage hybrid isolated dc–dc boost converter for high power and wide input voltage range applications," *IEEE Trans. Ind. Electron.*, vol. 69, no. 7, pp. 6751–6763, Jul. 2022.
[12] G. Wen, Y. Chen, Z. Zhong, and Y. Kang, "Dynamic voltage and current assignment strategies of nine-switch-converter-based DFIG wind power system for low-voltage ride-through (LVRT) under symmetrical grid voltage dip," *IEEE Trans. Ind. Appl.*, vol. 52, no. 4, pp. 3422–3434, Jul./Aug. 2016.
[13] D. Mishra, B. Singh, and B. K. Panigrahi, "Adaptive current control for a bidirectional interleaved EV charger with disturbance rejection," *IEEE Trans. Ind. Appl.*, vol. 57, no. 4, pp. 4080–4090, Jul./Aug. 2021.
[14] L. Tan, B. Wu, V. Yaramasu, S. Rivera, and X. Guo, "Effective voltage balance control for bipolar-dc-bus-fed EV charging station with three-level dc–dc fast charger," *IEEE Trans. Ind. Electron.*, vol. 63, no. 7, pp. 4031–4041, Jul. 2016.
[15] D. Cittanti, M. Gregorio, E. Vico, F. Mandrile, E. Armando, and R. Bojoi, "High-performance digital multiloop control of LLC resonant converters for EV fast charging with LUT-based feedforward and adaptive gain," *IEEE Trans. Ind. Appl.*, vol. 58, no. 5, pp. 6266–6285, Sep./Oct. 2022.
[16] Z. Liang et al., "A comprehensive, practical and reliable soft start-up and shut-down schemes for a multi-function integrated EV charger," in *Proc. IEEE Energy Convers. Congr. Expo.*, 2023, pp. 2718–2724.
[17] N.-D. Nguyen, C. Yoon, and Y. I. Lee, "A standalone energy management system of battery/supercapacitor hybrid energy storage system for electric vehicles using model predictive control," *IEEE Trans. Ind. Electron.*, vol. 70, no. 5, pp. 5104–5114, May 2023.
[18] N. Hou, L. Ding, P. Gunawardena, Y. Zhang, and Y. W. Li, "A comprehensive comparison of two fast-dynamic control structures for the DAB dc–dc converter," *IEEE Trans. Power Electron.*, vol. 37, no. 6, pp. 6488–6500, Jun. 2022.
[19] F. An et al., "Improved dynamic performance of dual active bridge dc–dc converters using MPC scheme," *IET Power Electron.*, vol. 11, no. 11, pp. 1756–1765, Sep. 2018.
[20] N. Hou, Y. Zhang, and Y. W. Li, "A natural transient-behavior-based control theory for DAB-based two-stage dc–dc converter," *IEEE Trans. Power Electron.*, vol. 38, no. 12, pp. 15137–15141, Dec. 2023.
[21] N. Hou, W. Song, and M. Wu, "Minimum-current-stress scheme of dual active bridge dc–dc converter with unified phase-shift control," *IEEE Trans. Power Electron.*, vol. 31, no. 12, pp. 8552–8561, Dec. 2016.
[22] W. Qian, H. Cha, F. Z. Peng, and L. M. Tolbert, "55-kW variable 3X dc-dc converter for plug-in hybrid electric vehicles," *IEEE Trans. Power Electron.*, vol. 27, no. 4, pp. 1668–1678, Apr. 2012.

Nie Hou (Member, IEEE) received the B.Sc. and M.Sc. degrees (Hons.) from Southwest Jiaotong University, Chengdu, China, in 2014 and 2017, respectively, and the Ph.D. degree from University of Alberta, Edmonton, AB, Canada, in 2022, all in electrical engineering.

He is currently a postdoctoral fellow with the University of Alberta. He authored or coauthored more than 50 refereed papers and holds 5 Chinese patents. His research interests include digital control and optimization methods of dc–dc converters and dc distribution systems.

Dr. Hou is a guest editor for *Applied Sciences and Electronics*, the topic chair with the 14th IEEE Energy Conversion Congress and Exposition, and the reviewing chair and the session chair with the 10th International Power Electronics and Motion Control Conference. He was the recipient of the Outstanding Author Award from the Proceeding of the Chinese Society for Electrical Engineering in 2016, the IAS Sustainable and Renewable Energy Conversion System Committee Conference Paper Awards in 2021, the Best Presenter at the 2nd International Power Electronics and Application Symposium in 2023, and the Best Special Session Chair Award at the 10th International Power Electronics and Motion Control Conference in 2024. He is recognized as 2022 World's Top 2% Scientists by Stanford University.

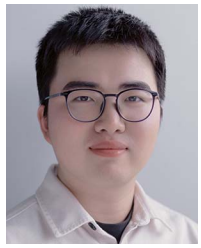

Kejun Qin (Student Member, IEEE) received the B.Eng. degree from Southwest Jiaotong University, Chengdu, China, in 2020, and the M.Sc. degree from Sichuan University, Chengdu, China, in 2023, both in electrical engineering. He is currently working toward the Ph.D. degree in energy systems with the Department of Electrical and Computer Engineering, University of Alberta, Edmonton, AB, Canada.

His research interests include dc circuit breakers and dual active bridge converters.

Ruizhi Wei (Student Member, IEEE) received the B.S. degree in electrical engineering from the Nanjing University of Science and Technology, Nanjing, China, in 2018, and the M.S. degree in electrical engineering from the Harbin Institute of Technology, Harbin, China, in 2020. He is currently working toward the Ph.D. degree in electrical engineering with the Department of Electrical and Computer Engineering, University of Alberta, Edmonton, AB, Canada.

His research interests include the control and optimization of bidirectional dc–dc converters and their applications.

Yue Zhang (Member, IEEE) received the B.Sc. and M.Sc. degrees from Nanjing University of Aeronautics and Astronautics, Nanjing, China, in 2012 and 2015, respectively, and the Ph.D. degree from Southeast University, Nanjing, China, in 2020, all in electrical engineering.

From 2017 to 2019, he was a visiting Ph.D. student with the University of Alberta, Edmonton, AB, Canada, where he is currently a postdoctoral fellow. His research interests include dc–dc converters and magnetic design.

Yun Wei Li (Fellow, IEEE) received the B.Sc. degree from Tianjin University, Tianjin, China, in 2002, and the Ph.D. degree from Nanyang Technological University, Singapore, in 2006, both in electrical engineering.

In 2015, he was a visiting scholar with Aalborg University, Aalborg, Denmark. From 2006 to 2007, he was a postdoctoral research fellow with Ryerson University, Toronto, ON, Canada. In 2007, he also worked with Rockwell Automation Canada Inc., before he joined the University of Alberta in the same year. Since then, he has been with the University of Alberta, where he is currently a Professor and Acting Department Chair. His research interests include distributed generation, microgrids, renewable energy, high-power converters, and electric motor drives.

Dr. Li is the Vice President for Products of IEEE Power Electronics Society. Before that, he was the Editor-in-Chief for the IEEE TRANSACTIONS ON POWER ELECTRONICS LETTERS, an Associate Editor for IEEE TRANSACTIONS ON POWER ELECTRONICS, IEEE TRANSACTIONS ON INDUSTRIAL ELECTRONICS, IEEE TRANSACTIONS ON SMART GRID, and IEEE JOURNAL OF EMERGING AND SELECTED TOPICS IN POWER ELECTRONICS. He was the General Chair of IEEE Energy Conversion Congress of Exposition in 2020. From 2021 to 2023, he was the AdCom Member with Large for IEEE Power Electronics Society. He is recognized as a Highly Cited Researcher by the Web of Science Group. He was selected as a Fellow of the Canadian Academy of Engineering in 2024. He was the recipient of the Richard M. Bass Outstanding Young Power Electronics Engineer Award from IEEE Power Electronics Society in 2013 and the 8th Nagamori Awards in 2022.